

# PCCP

Accepted Manuscript



This is an *Accepted Manuscript*, which has been through the Royal Society of Chemistry peer review process and has been accepted for publication.

*Accepted Manuscripts* are published online shortly after acceptance, before technical editing, formatting and proof reading. Using this free service, authors can make their results available to the community, in citable form, before we publish the edited article. We will replace this *Accepted Manuscript* with the edited and formatted *Advance Article* as soon as it is available.

You can find more information about *Accepted Manuscripts* in the [Information for Authors](#).

Please note that technical editing may introduce minor changes to the text and/or graphics, which may alter content. The journal's standard [Terms & Conditions](#) and the [Ethical guidelines](#) still apply. In no event shall the Royal Society of Chemistry be held responsible for any errors or omissions in this *Accepted Manuscript* or any consequences arising from the use of any information it contains.

# The conjugated oligoelectrolyte DSSN+ enables exceptional coulombic efficiency *via* direct electron transfer for anode-respiring *Shewanella oneidensis* MR-1—a mechanistic study†

By Cite this: DOI: 10.1039/x0xx00000x

Received 00th January 2012,  
Accepted 00th January 2012

DOI: 10.1039/x0xx00000x

www.rsc.org/

Nathan D. Kirchhofer,<sup>a</sup> Xiaofen Chen,<sup>b</sup> Enrico Marsili,<sup>c</sup> James J. Sumner,<sup>d</sup>  
Frederick W. Dahlquist,<sup>b,\*</sup> Guillermo C. Bazan<sup>a,b,e,\*</sup>

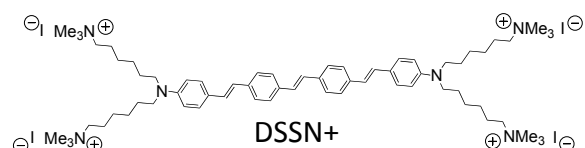
*Shewanella oneidensis* MR-1 was cultivated on lactate with poised graphite electrode acceptors ( $E = +0.2$  V vs. Ag/AgCl) in order to explore the basis for sustained increases in anodic current output following addition of the lipid-intercalating conjugated oligoelectrolyte (COE) 4,4'-bis(4'-(*N,N*-bis(6''-(*N,N,N*-trimethylammonium)hexyl)amino)-styryl)stilbene tetraiodide (DSSN+). Microbial cultures spiked with DSSN+ exhibit a ~2.2-fold increase in charge collected, a ~3.1-fold increase in electrode colonization by *S. oneidensis*, and a ~1.7-fold increase in coulombic efficiency from  $51 \pm 10\%$  to an exceptional  $84 \pm 7\%$  without obvious toxicity effects. Direct microbial biofilm voltammetry reveals that DSSN+ rapidly, sustainably increases cytochrome-based direct electron transfer and subsequently increases flavin-based mediated electron transfer. Control experiments indicate that DSSN+ does not contribute to current in the absence of bacteria.

**Broader Impact:** The conversion of organic carbon substrates to electricity by exoelectrogenic bacteria such as *Shewanella oneidensis* MR-1 is of relevance for its potential utility in wastewater treatment, environmental remediation, and power generation for remote sensing. However, direct conversion of organic carbon to electricity remains slow and inefficient with respect to other bioconversion processes. The efficiency of the process is usually measured by the coulombic efficiency (CE) of the system, which is the percentage of the theoretical maximum charge that the system produces from a given quantity of substrate. This contribution demonstrates that modifying anodic *S. oneidensis* with the conjugated oligoelectrolyte DSSN+ induces exceptional coulombic efficiency in conversion of lactate to electricity as well as striking increases in anodic current, or electron transfer rate. Voltammetric analysis provides direct, quantitative evidence that DSSN+ primarily boosts direct electron transfer to an electrode. This is a vital conceptual steppingstone in designing synthetic modifications of biotic-abiotic electronic interfaces.

*Shewanella oneidensis* MR-1 is a dissimilatory metal-reducing bacterium capable of respiring on a variety of soluble and insoluble acceptors.<sup>1–4</sup> This species is capable of anaerobic growth<sup>5</sup> by transporting electrons across its outer membrane *via* the MtrCAB-OmcA porin-cytochrome complex<sup>6</sup> to respire on exogenous metal oxides and electrodes, producing usable electrical current in the latter case. From the standpoint of bioelectricity production, which has applications in, for example, improving wastewater treatment or autonomous remote sensing systems, it is desirable to increase the coulombic efficiency (CE) as much as possible, and this challenge is under study in bioelectronics<sup>7</sup> and electromicrobiology.<sup>8–10</sup>

Key extracellular electron transport (EET) processes proposed<sup>11</sup> in *S. oneidensis* include (1) direct electron transfer (DET) to solid-state acceptors *via* terminal membrane-bound cytochromes MtrC and OmcA,<sup>12–20</sup> and (2) mediated electron transfer (MET) by secreted flavin-based molecules that shuttle electrons between cytochromes and exogenous acceptors,<sup>16,21–25</sup> as well as increase the electron transfer rate as bound flavin semiquinone.<sup>26–28</sup> These EET processes are electrochemically distinguishable in characteristic redox potential ranges of  $-0.4$ - $0$  V (MET) and  $0$ - $0.2$  V (DET)<sup>11</sup> which provides a crucial mechanistic backdrop for assessing perturbations to EET. A bottleneck exists for DET in the final electron transfer step to the solid acceptor<sup>16</sup> because MtrC and OmcA must come into intimate contact with the surface. Flavins may alleviate this barrier by coming into diffusive contact with MtrC and OmcA.<sup>27–29</sup> Finally, a third respiratory process has been discussed involving electrically conductive biosynthesized “nanowires” that transport electrons *via* DET over long distances,<sup>30–35</sup> and this mechanism remains under investigation.<sup>36,37</sup>

Conjugated oligoelectrolytes (COEs), such as 4,4'-bis(4'-(*N,N*-bis(6''-(*N,N,N*-trimethylammonium)hexyl)amino)-styryl)stilbene



tetraiodide (DSSN<sup>+</sup>), have recently drawn attention for their ability to increase current production in microbial fuel cells with *S. cerevisiae*,<sup>38</sup> *E. coli*,<sup>39,40</sup> and wastewater,<sup>41</sup> as well as current-driven substrate turnover in *S. oneidensis* microbial electrosynthesis cells.<sup>42</sup> Optical characterization indicates that DSSN<sup>+</sup> intercalates into membranes perpendicular to their surface.<sup>38,39,42,43</sup> Additional studies indicate that intercalated DSSN<sup>+</sup> can promote fluorescence resonance energy transfer<sup>44</sup> and transmembrane ion conductance<sup>45</sup> with minimal membrane perturbation.<sup>46</sup> Most recently, studies with *S. oneidensis* MR-1 indicate that supplemented flavin provides a higher-magnitude current boost than DSSN<sup>+</sup>, and yet DSSN<sup>+</sup> does appear to decrease charge transfer resistance independently of flavin.<sup>47</sup> However, detailed understanding of the mechanism of EET enhancement was not provided in that study, nor was any quantitative correlation made to device efficiency or biomass. These essential, missing elements are presented here.

In this contribution, the impact of DSSN<sup>+</sup> addition to *S. oneidensis* EET is examined through use of 3-electrode batch-type membraneless bioelectrochemical reactors. The resulting data provide direct evidence that rapid, sustainable increases in anodic respiratory current and the exceptionally-high CE from DSSN<sup>+</sup> addition arise from (1) an increase in cytochrome-based DET redox current and (2) an increase in biofilm formation on the electrode, which together also increase the flavin-based MET redox current over time.

In this work, triplicate unmodified control reactors (hereafter referred to as "Type 1") are statistically compared to identically prepared triplicate test reactors that receive 5 μM DSSN<sup>+</sup> during operation (hereafter referred to as "Type 2"). For each reactor, chronoamperometry (CA), cyclic voltammetry (CV), and differential pulse voltammetry (DPV) were conducted. For clarity throughout the text, the same single representative experiment is presented in figures to showcase the discussed behavior of the reactors. Average parameters from triplicate reactors are presented in Table 1 and additional data is provided in the Electronic Supplementary Information (ESI) as indicated in the text. It is important to note that reported current densities in these experiments are calculated for 1 cm × 1 cm × 0.2 cm carbon felt working electrodes with a surface area of 226 ± 12 cm<sup>2</sup>, as described in the ESI. This surface area is ~81-fold larger than had been previously reported for identical electrodes,<sup>47</sup> so current densities herein are accordingly ~81-fold smaller.

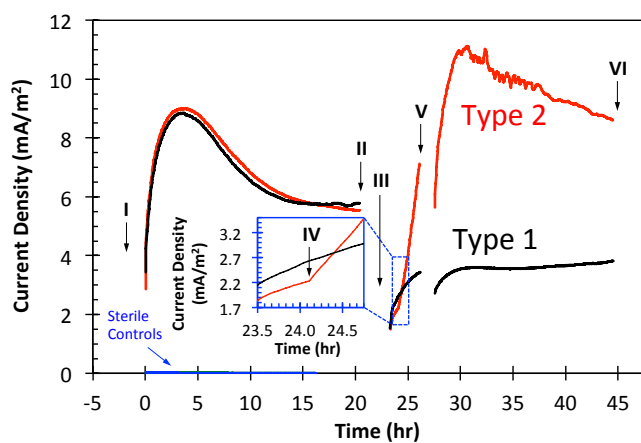


**Figure 1.** Representative CA from one replicate of *S. oneidensis* in modified M1 minimal media at a poised potential of  $E = +0.2$  V vs. Ag/AgCl reaffirms a rapid, sustained current increase upon addition of DSSN<sup>+</sup>. Note negligible current output from sterile controls (additional details may be found in ESI). (I) Inoculation of reactors and initiation of current collection. (II) Full media change; reactor volume was replaced with fresh M1 media containing 30 mM Na-(L)-lactate. (III) HPLC sample, CV, and DPV after the full media change; CA resumed. (IV, inset) Addition of 5 μM DSSN<sup>+</sup> to Type 2 reactor. (V) CV and DPV ~2 hours after DSSN<sup>+</sup> addition to examine the electrochemical nature of the current acceleration. (VI) HPLC sample, CV, and DPV at the end of current collection, followed by chemical cell fixation and SEM of the fixed electrode.

Fig. 1 displays the CA results as a function of time for the two types of reactors. Also shown are relevant timepoints in the course of the experiments; these are designated I to VI. The data from I to II ( $t = 0$ – $20.4$  h) compares the current generation for the two reactors, prior to DSSN<sup>+</sup> addition to Type 2 reactors; during this time, one observes virtually identical behavior between the two biofilms. After the full medium change at II, all reactors typically reduce their current output to about 40% of the maximum observed between I and II. This is due to removal of planktonic cells and extracellular flavins that contribute to anodic current,<sup>23,47</sup> leaving only the biofilm to produce current.

Examination of Fig. 1 from III ( $t = 23.2$  h) to VI ( $t = 44.5$  h) shows that when DSSN<sup>+</sup> is added to Type 2 reactors at IV ( $t = 24.1$  h), an acceleration in current production occurs within a short time ( $\leq 160$  seconds), while Type 1 reactors remain stable. This  $\leq 160$  second response is much faster than the ~1.5 hour generation time of *S. oneidensis* in minimal media,<sup>48</sup> suggesting a boost in EET and not stimulated growth. After IV, current output from the Type 2 reactors

Table 1. Triplicate Mean Parameters and Normalized Ratios from Type 1 and Type 2 Reactors

Parameter	Expression	Type 1 Reactor	Type 2 Reactor	$p$ -value <sup>e</sup>	Normalized Ratio (Type 2:Type 1) <sup>f</sup>
Biofilm Collected Charge (C) <sup>a</sup>	$Q_{III-VI} = \int I_{III-VI}(t) dt$	5.2 ± 0.9	11.4 ± 2.7	0.036	2.2 ± 0.4
[lactate] Change (mM) <sup>a</sup>	$\Delta[\text{lac}]$	-1.8 ± 0.2	-2.3 ± 0.4	0.251	1.3 ± 0.4
Ideal Charge Collected (C) <sup>a,b</sup>	$Q_{ideal} = -\Delta[\text{lac}] \times VFz$	10.4 ± 1.2	13.5 ± 2.4	0.251	1.3 ± 0.4
Coulombic Efficiency (%) <sup>a</sup>	$CE = 100 \times Q_{III-VI}/Q_{ideal}$	51 ± 10	84 ± 7	0.010	1.7 ± 0.3
Electrode Cell Density (million/cm <sup>2</sup> ) <sup>c</sup>	$\rho = (1/12) \sum_{i=1}^{12} (N_i/\pi d_i h)$	23 ± 10	70 ± 25	0.120	3.1 ± 0.6
Max Current per Unit Dry Cell Mass (μA/mg) <sup>d</sup>	$I_{III-VI}(max)/\rho A_{electrode} m$	44 ± 9	34 ± 4	0.119	0.8 ± 0.2

a. After media change to end of operation (between III and VI), thus deconvoluting the biofilm signal from bulk solution

b. Calculated assuming 100% CE ( $z = 4$  electrons/lactate);  $V$  = reactor volume (15 mL);  $F$  = Faraday constant =  $N_A e$

c. At the end of reactor operation (timepoint VI); values are mean ± std. dev. ( $k = 12$  replicates for each of 3 electrodes of each type)

d. Surface area of the graphite felt electrodes,  $A_{electrode}$ , was determined to be 226 ± 12 cm<sup>2</sup> ( $k = 24$  replicates). The specific mass of  $1 \times 10^6$  cells,  $m$ , was determined to be  $4.4 \pm 0.6 \times 10^{-7}$  g ( $k = 3$  replicates).  $I_{III-VI}(max)$  was extracted from CA data. See ESI, Methods, for details.

e. Calculated from 2-tailed  $t$ -tests. If four decimal places were retained, the  $p$ -value for CE is 0.0098 (i.e. > 99% significance)

f. Normalized Ratios are calculated by first dividing the parameter values for each reactor by  $Q_{I-II}$  (i.e. integrated total charge collected between I and II) and then calculating the ratio. This treatment numerically corrects for possible confounding differences in the geometry and absolute number of cells on the electrode during biofilm establishment. For Electrode Cell Density, uncertainty was propagated by addition in quadrature to determine the std. dev.

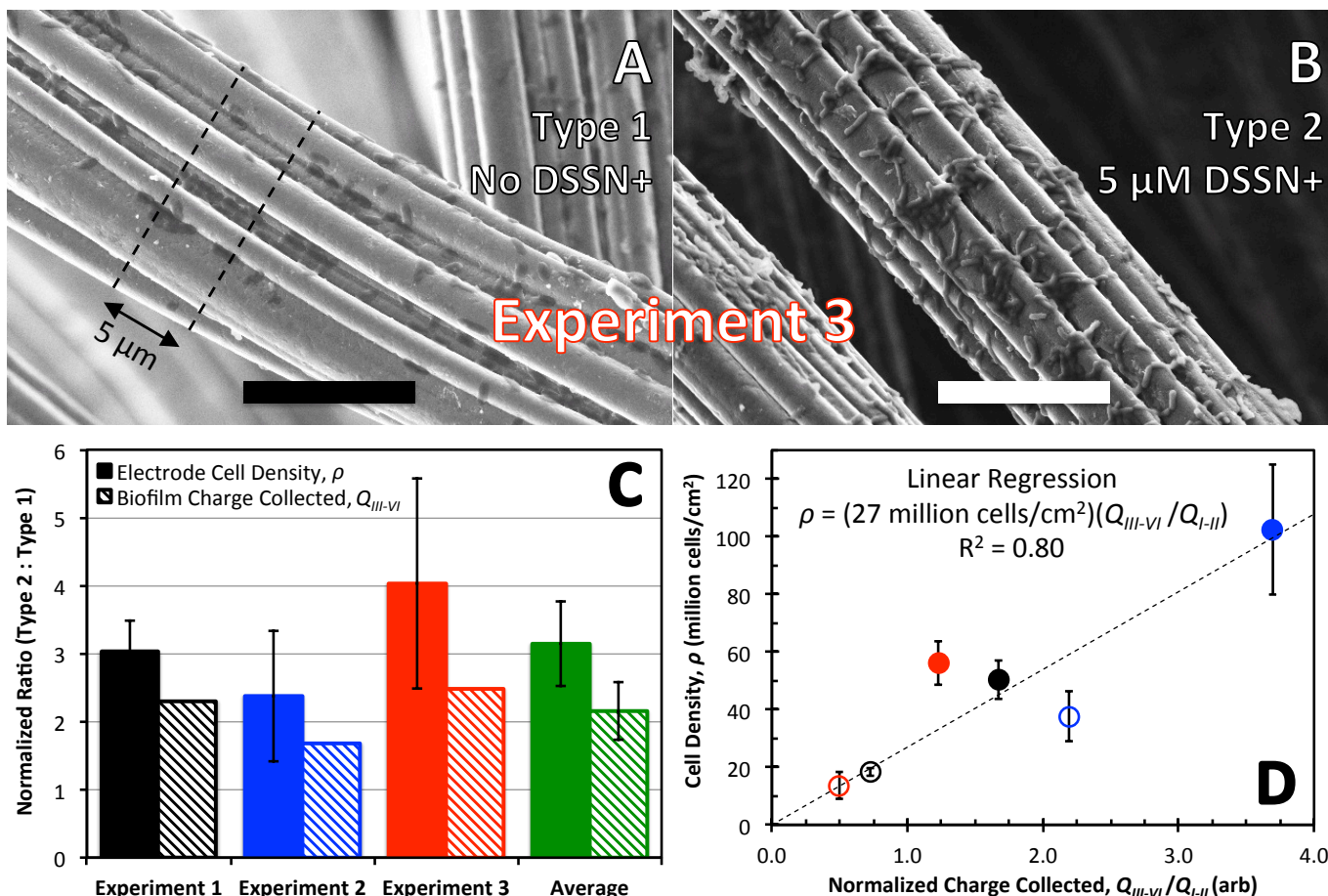


**Figure 2.** Representative SEM images of chemically fixed graphite felt working electrodes, summary of resulting electrode cell density measurements, and correlation to biofilm collected charge. All six electrodes were imaged after timepoint VI, but only images from Experiment 3 are presented for clarity. Scale bars are 10  $\mu\text{m}$ . (A) Fixed working electrode from **Type 1** reactor. Dashed lines illustrate a possible geometric section utilized for cell counting. (B) Fixed working electrode from **Type 2** reactor. (C) Normalized Ratios of Electrode Cell Density,  $\rho$ , and Biofilm Collected Charge,  $Q_{III-VI}$ , between all **Type 2** and **Type 1** reactors in this study. Green bars: average of Experiments 1, 2, and 3. Additional SEM images can be found in ESI, Fig. S3, and details of normalization can be found in Table 1, f. (D) Plot of Electrode Cell Density,  $\rho$ , vs. Normalized Charge Collected,  $Q_{III-VI}/Q_{I-III}$ , for all six reactors in this work. Black, Experiment 1; Blue, Experiment 2; Red, Experiment 3; Open circles, **Type 1** reactors; Closed circles, **Type 2** Reactors; Dashed line, best-fit linear regression (equation inset).

remains  $\geq 2$ -fold higher than **Type 1** reactors, indicating the enhancement is sustained (see Fig. S1 for the other two replicates).

From III to VI, DSSN+ addition also induces a statistically significant  $\sim 1.7 \pm 0.3$ -fold increase in the CE ( $p = 0.010$ ) from  $51 \pm 10\%$  (**Type 1** reactors) to  $84 \pm 7\%$  (**Type 2** reactors). The latter value is extraordinarily high for *S. oneidensis*-based devices.<sup>49</sup> Biofilm collected charge,  $Q_{III-VI}$ , also statistically significantly increases  $2.2 \pm 0.4$ -fold ( $p = 0.036$ ) from  $5.2 \pm 0.9$  C (**Type 1**) to  $11.4 \pm 2.7$  C (**Type 2**) during this time. Table 1 provides a summary of all data relevant to these measurements, including lactate concentration change,  $\Delta[\text{lac}]$ , and ideal charge collected from that lactate consumption,  $Q_{ideal}$ . Normalized ratios  $\pm$  standard deviations as well as  $p$ -values for these parameters comparing **Type 2** and **Type 1** reactors are also provided, and indicate that not all measured parameters change statistically significantly with DSSN+ addition. It is also worth mentioning that in sterile reactors with poised electrodes containing growth media, DSSN+, and/or lactate, anodic current is negligibly small compared to reactors with *S. oneidensis* (this data is presented in Fig. 1, but for clarity can also be found in Fig. S2). Therefore, addition of DSSN+ and lactate has no current-enhancing effect in the absence of cells.

At the end of operation, electrodes were removed, chemically

fixed, and sliced with a razor for SEM imaging to estimate the electrode surface cell density,  $\rho$  (Fig. 2 A,B). Details of calculation of  $\rho$  are provided in the ESI, and SEM images from remaining replicate experiments are found in Fig. S3. For **Type 1** reactors (Fig. 2A), triplicate average cell density is  $\rho = 2.3 \pm 1.0 \times 10^7$  cells/cm<sup>2</sup>, whereas for the **Type 2** reactors (Fig. 2B) one observes  $\rho = 7.0 \pm 2.5 \times 10^7$  cells/cm<sup>2</sup>. These images thus demonstrate a  $3.1 \pm 0.6$ -fold increase in  $\rho$  for **Type 2** reactors compared to **Type 1** ( $p = 0.120$ ). Such features are summarized in Fig. 2 C,D and are provided in Table 1. This set of experiments demonstrates that DSSN+ promotes electrode colonization and confirms that the addition of 5  $\mu\text{M}$  DSSN+ is not toxic to the developing biofilm. It is also notable that the planktonic turbidity remains undetectable during this time. Comparison of the  $\rho$ -increase ( $3.1 \pm 0.6$ ) and the  $Q_{III-VI}$ -increase ( $2.2 \pm 0.4$ ) indicates that DSSN+ does not improve EET on a per-cell basis. However, one finds a linear relationship (Fig. 2D) between  $\rho$  and the normalized charge collected,  $Q_{III-VI}/Q_{I-III}$ , which shows that DSSN+-induced increases are not reactor-specific (see Table 1 for normalization details).

At timepoints III, V, and VI in Fig. 1, current collection was paused to conduct CV and DPV experiments. CV measurements at these timepoints (Fig. 3 A,C) reveal two primary reversible catalytic electron

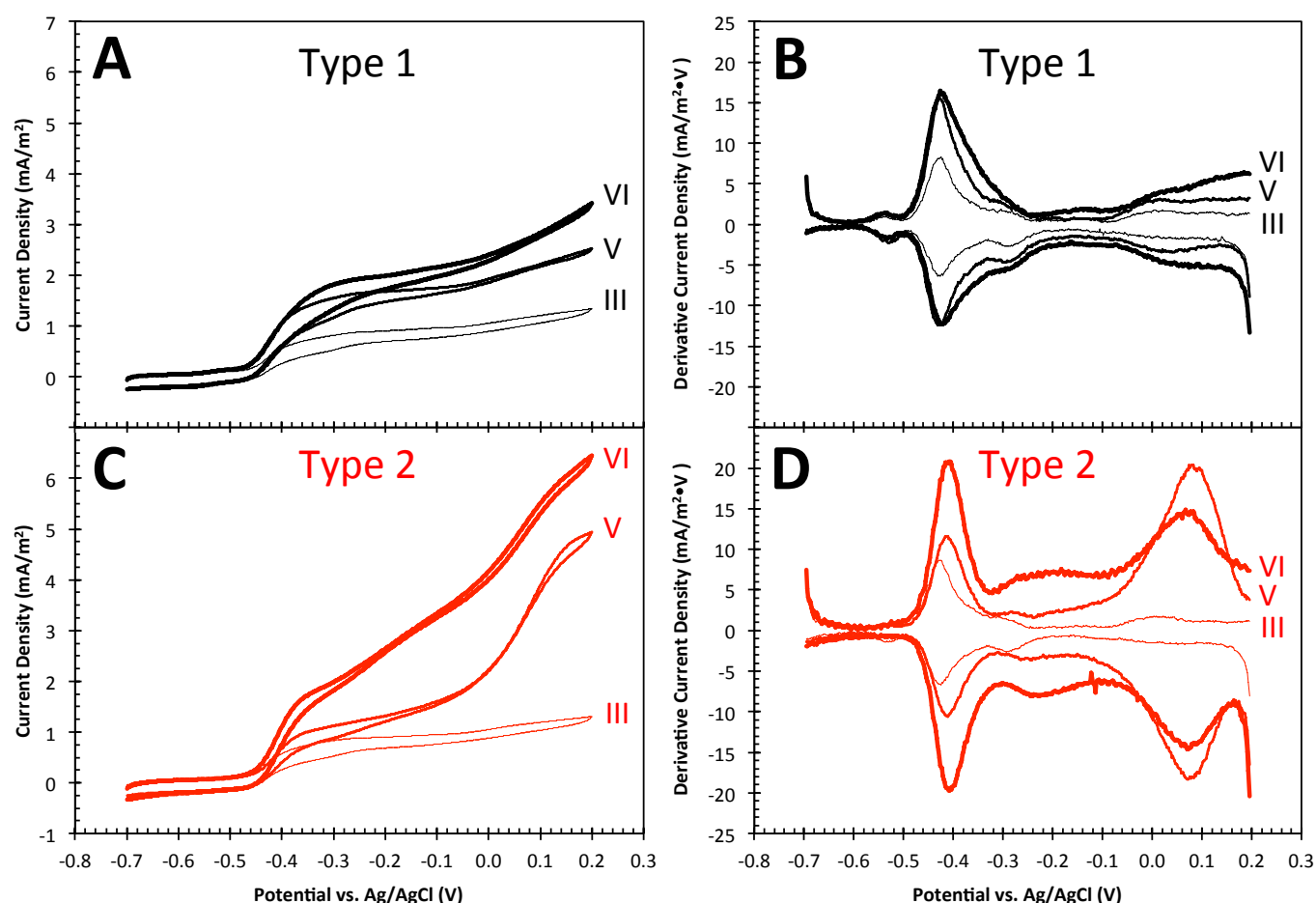


**Figure 3.** Representative turnover CV and first derivative traces for **Type 1** and **Type 2** reactors to identify redox species affected by addition of DSSN+. All scans were conducted at 5 mV/s at timepoints III, V, and VI. The additional two replicate experiments are presented in Fig. S1. (A) CV traces from the **Type 1** reactor. (B) 1st derivative of CV traces from the **Type 1** reactor. (C) CV traces from the **Type 2** reactor. (D) 1st derivative of CV traces from the **Type 2** reactor.

transfer waves as the potential is swept past  $E = -0.42$  V and  $0.05$  V. That is, current output at these two potentials rises rapidly and begins to saturate at a limiting current, which is characteristic of redox species rapidly cycling back to a reduced state from metabolic turnover, thereby continuously supplying the electrode with electrons.<sup>50,51</sup> The absence of local maxima in the current response indicates no lactate mass transport limitations. Potentials of  $-0.42$  V and  $+0.05$  V are assigned to MET via flavins<sup>21,22</sup> and DET via cytochromes,<sup>11,28,52</sup> respectively. Additionally, it is worth noting that the current produced at the CV vertex potential ( $E = +0.2$  V) at III, V, and VI in Fig. 3 A,C is similar in amplitude to the CA current at the same timepoints in Fig. 1, indicating that the electrochemical analyses accurately interrogate the respiring biofilms.

From first derivative analysis of the CV traces (Fig. 3 B,D), an additional catalytic wave can be detected near  $E = -0.3$  V. This redox feature is tentatively assigned to flavin semiquinone based on the similarity to the previously reported biologically-stabilized flavin semiquinone peak position.<sup>28,53</sup> CV studies of sterile M1 media containing riboflavin, lactate, and/or DSSN+ (Fig. S4) lack this redox peak, further suggesting it is biologically-stabilized. Derivative analysis also reveals a redox feature at  $E = -0.54$  V which does not contribute to catalytic electron transfer and is associated with the media (assigned by its presence in Fig. S4). Finally, Fig. S4 also

indicates that DSSN+ is not redox active in the aqueous media in the potential window used for voltammetry ( $-0.7$  V  $< E < +0.2$  V) and therefore does not contribute to current.

In Fig. 3, it becomes apparent that the EET increase from DSSN+ addition in the **Type 2** reactor arises from current through the cytochrome DET machinery ( $E > -0.1$  V<sup>11</sup>). This can be observed readily at timepoints V and VI by comparing the large-amplitude peak at  $E = +0.05$  V in Fig. 3D to the same peak in Fig. 3B (the **Type 1** reactor). Enhanced DET is consistent with the observed increase in CE, as DET is reported to be more efficient than MET due to diffusive loss of electrons in the latter.<sup>49</sup> Additionally, the elevated DET appears to cause a subsequent delayed increase of flavin signals over the same time period, seen by the increase in CV derivative peak amplitudes for flavin and flavin semiquinone at  $E = -0.42$  V and  $-0.3$  V, respectively, by timepoint VI (Fig. 3D).<sup>28,29</sup> An additional set of control CV experiments was conducted with the reactors' effluent after timepoint VI in freshly autoclaved identical reactors (Fig. S5). These experiments show essentially no faradaic current and hence indicate that nearly all of the electroactivity in Figs. 1–3 arises from electrode-associated cells. Thus, the media change at II is effective in deconvoluting the biofilm signal from any bulk solution contributions.

DPV measurements (Fig. 4) were conducted immediately following CV analyses. These experiments are qualitatively similar to

the first derivative CV analyses of the electrodes, but DPV provides resolution by subtracting non-faradaic current from the redox signals.<sup>56</sup> Additionally, with mathematical modelling, peak areas empirically correlate to effective surface concentrations of redox species, and peak widths empirically correlate to the number of electrons transferred per redox reaction,  $n^{56}$  (see ESI, **Methods** for details). In this section, representative data from Experiment 3 is presented as well as numerically summarized in **Table 2**.

First, DPV redox peaks in the **Type 1** reactor were analysed to establish values for an unmodified reactor (**Fig. 4A**). The area under the  $E = +0.05$  V cytochrome peak increases over time. Fitting and integration of this peak (**Fig. S6**) reveals that the concentration increases by 2.3-fold ~3 hours after the media change (**Fig. 4A, V**) and continues to increase by up to 3.5-fold at the end of reactor operation (**Fig. 4A, VI**). Similar analysis of the  $E = -0.3$  V (flavin semiquinone) and  $E = -0.42$  V (flavin) peaks indicates that flavin semiquinone concentration increases only marginally (by 1.1-fold) ~3 hours after the media change (**V**) and stays at the same level (no obvious increase) until the end of reactor operation (**VI**). Flavin concentration increases by 1.7-fold approximately 3 hours after the media change (**V**), staying at the same level until the end of reactor operation (**VI**).

Next, DPV redox peaks in the **Type 2** reactor (**Fig. 4B**) were analysed for comparison to the **Type 1** reactor. Cytochrome concentration increases by 9.3-fold ~2 hours after DSSN+ addition (**V**), and then falls off to a 6.2-fold increase at the end of reactor operation (**VI**); the latter is nearly a 2-fold increase compared to the **Type 1** reactor, and represents a quantitative measure of DSSN+ enhancing the rate of DET. Increases in concentrations of flavin semiquinone and flavin lag this increase in cytochrome signal. Flavin semiquinone increases negligibly ~2 hours after DSSN+ addition (**V**), but eventually increases by up to 1.7-fold at the end of reactor operation (**VI**)—much higher than the **Type 1** reactor, and consistent with an increased rate of electron transfer.<sup>28</sup> Flavin increases by 1.4 fold ~2 hours after DSSN+ addition (**V**), which is reduced 0.3-fold compared to the **Type 1** reactor at the same point. Ultimately, flavin increases 3.4-fold by the

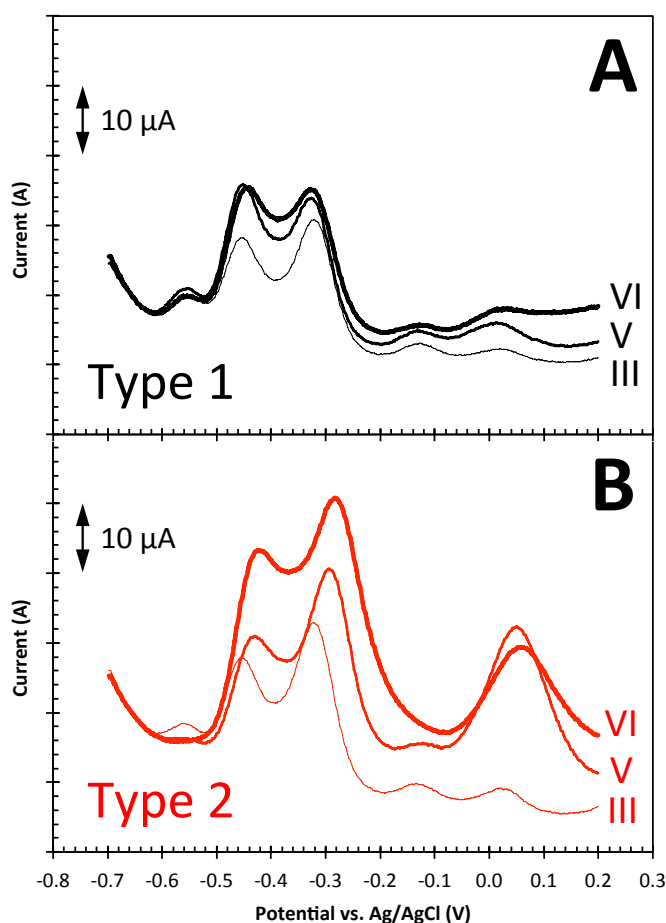


**Figure 4.** DPV scans of working electrodes from representative **Type 1** and **Type 2** reactors show substantial increases in DET (and subsequently MET) redox activity due to DSSN+ addition. Scan rate matches CV at 5 mV/s for the most direct comparison. Note the 10  $\mu$ A scaling arrow for the vertical axis (not current density). (A) Scans of the **Type 1** reactor at timepoints III, V, and VI. (B) Scans of **Type 2** reactor at timepoints III, V, and VI.

**Table 2.** Extracted Redox Parameters from Gaussian Fits to DPV Peaks from Representative Type 1 and Type 2 Reactors

Redox Species	Extracted DPV Redox Parameter	Variable	Type 1 Reactor			Type 2 Reactor		
			III	V	VI	III	V	VI
Flavin	Peak Center (V vs. Ag/AgCl) <sup>a</sup>	$E_o$	-0.428	-0.426	-0.416	-0.430	-0.404	-0.398
	Peak Height ( $\mu$ A) <sup>a</sup>	$I_o$	10.8	18.2	18.1	10.9	15.3	27.5
	Peak FWHM (mV)	$2.35\sigma$	71	71	71	71	71	94
	$e^-$ Transferred per Redox Reaction <sup>b</sup>	$n = 2.30RT/\sigma F$	2.0	2.0	2.0	2.0	2.0	1.5
	Peak Area ( $\mu$ A·mV)	$\int I(E)dE$	814	1369	1363	820	1154	2754
	Normalized Concentration <sup>c</sup>	—	1.0	1.7	1.7	1.0	1.4	3.4
Flavin semiquinone	Peak Center (V vs. Ag/AgCl) <sup>a</sup>	$E_o$	-0.298	-0.304	-0.304	-0.298	-0.270	-0.258
	Peak Height ( $\mu$ A) <sup>a</sup>	$I_o$	19.6	21.0	20.6	25.4	25.8	33.6
	Peak FWHM (mV)	$2.35\sigma$	94	94	94	94	94	118
	$e^-$ Transferred per Redox Reaction <sup>b</sup>	$n = 2.30RT/\sigma F$	1.5	1.5	1.5	1.5	1.5	1.2
	Peak Area ( $\mu$ A·mV)	$\int I(E)dE$	1964	2104	2065	2548	2595	4220
	Normalized Concentration <sup>c</sup>	—	1.0	1.1	1.1	1.0	1.0	1.7
DET (Cytochromes)	Peak Center (V vs. Ag/AgCl) <sup>a</sup>	$E_o$	0.047	0.037	0.061	0.047	0.075	0.083
	Peak Height ( $\mu$ A) <sup>a</sup>	$I_o$	2.0	3.5	3.5	3.8	21.1	12.7
	Peak FWHM (mV)	$2.35\sigma$	71	94	141	71	118	130
	$e^-$ Transferred per Redox Reaction <sup>b</sup>	$n = 2.30RT/\sigma F$	2.0	1.5	1.0	2.0	1.2	1.1
	Peak Area ( $\mu$ A·mV)	$\int I(E)dE$	149	348	522	284	2645	1748
	Normalized Concentration <sup>c</sup>	—	1.0	2.3	3.5	1.0	9.3	6.2

a.  $E_o$  values are corrected by one half the pulse height,  $\Delta E/2 = +25$  mV, and  $I_o$  values are baseline subtracted (see ESI for details)

b. Values of  $n$  are calibrated to the known 2-electron redox system of flavin using the FWHM (see ESI for details)

c. In all cases, concentration is reported normalized to the DPV-determined value at timepoint III, and is thus unitless

end of reactor operation (VI), which is a much larger increase than is observed in the **Type 1** reactor (1.7-fold). These DPV comparisons of the three redox species are consistent with the same trends in CV experiments in which DSSN+ increases cytochrome DET catalytic current in **Type 2** reactors (Fig. 3 A,C) and causes a subsequent delayed increase in the flavin-based MET catalytic currents. It is noteworthy that the rise in cytochrome DET signal is consistent with the observed growth in electrode-associated organisms in **Type 2** reactors (Fig. 2).

Okamoto *et al.*<sup>8</sup> suggested that the number of transferred electrons per redox reaction,  $n$ , changes from 2 to 1 when flavins bind to cytochromes of *S. oneidensis* in the semiquinone state, and that this improves the rate of EET for the respiring organism. To explore whether such a phenomenon contributes to DSSN+'s electron transfer boost, the full width at half maximum of DPV current peaks was used to extract reasonable values for  $n$ . Specifically, DSSN+ causes the flavin peak to shift from  $n = 2$  to  $n = 1.5$ , the flavin semiquinone peak to shift from  $n = 1.5$  to  $n = 1.2$ , and the cytochrome peak to shift from  $n = 2$  to  $n = 1.2$ , eventually reaching  $n = 1.1$ . These values are in contrast to the **Type 1** reactor where flavin and flavin semiquinone remain constant at  $n = 2$  and  $n = 1.5$ , respectively, and the cytochrome peak shifts from  $n = 2$  to  $n = 1.5$ , eventually reaching a value of  $n = 1$ . Fractional values of  $n$  may be rationalized by the fact that measurements represent a bulk average. This analysis shows that DSSN+ causes  $n$  to shift towards 1 for flavins, flavin semiquinones, and cytochromes, as evidenced by broadening of respective DPV current peaks in the **Type 2** reactors (see Table 2). A smaller  $n$  is consistent with the proposed EET rate enhancement and thus is also directly consistent with the observed increase in anodic current.

In summary, the addition of 5  $\mu\text{M}$  DSSN+ to poised *S. oneidensis* MR-1 bioreactors causes a rapid ( $\leq 160$  seconds), sustained current increase which results in a  $>2$ -fold increase in charge collected, a  $>3$ -fold increase in electrode colonization, and increases the CE of reactors from  $51 \pm 10\%$  to  $84 \pm 7\%$ —exceptionally high for a *S. oneidensis* device. Direct biofilm voltammetry indicates quantitatively that this EET increase from adding DSSN+ occurs *via* native cytochrome-based DET machinery and is consistent with respiration shifting towards a faster 1-electron process for all redox species involved. Because of their amphiphilic structure, COEs such as DSSN+ might physically access the comparably amphiphilic membrane-bound cytochromes OmcA and MtrC through electrically-insulating extracellular polymeric substances.<sup>55,56</sup> In this way, the aromatic core of the COE might effectively increase electronic surface area of the cytochromes and explain the rapid, sustainably-elevated rise in DET redox current.

## Acknowledgements

Funding was provided by the Institute for Collaborative Biotechnologies (ICB) under grant W911F-09-D-0001 from the U.S. Army Research Office. Content does not necessarily reflect the position or the policy of the Government, and no official endorsement should be inferred. Microscopy was conducted in MRL Shared Experimental Facilities at UCSB, which is supported by the MRSEC Program (NSF DMR 1121053), a member of the NSF-funded Materials Research Facilities Network.

## Notes and references

<sup>a</sup> Department of Materials, University of California, Santa Barbara, California, CA 93106, USA. Email: bazan@chem.ucsb.edu

<sup>b</sup> Department of Chemistry and Biochemistry, University of California, Santa Barbara, CA 93106, USA. Email: dahlquist@chem.ucsb.edu

<sup>c</sup> Marine and Environmental Sensing Technology Hub, Dublin City University, Dublin 9, Ireland

<sup>d</sup> Sensors and Electron Devices Directorate, U.S. Army Research Laboratory, Adelphi, Maryland 20783, USA

<sup>e</sup> Center of Excellence for Advanced Materials Research (CEAMR), King Abdulaziz University, Jeddah, Saudi Arabia

† Electronic Supplementary Information (ESI) available: Full Methods as well as figures, captions, and discussion of data from replicate reactors and sterile control experiments. See DOI: 10.1039/b000000x/

1. J. F. Heidelberg, I. T. Paulsen, K. E. Nelson, E. J. Gaidos, W. C. Nelson, T. D. Read, J. A. Eisen, R. Seshadri, N. Ward, B. Methe, R. A. Clayton, T. Meyer, A. Tsapin, J. Scott, M. Beanan, L. Brinkac, S. Daugherty, R. T. DeBoy, R. J. Dodson, a S. Durkin, D. H. Haft, J. F. Kolonay, R. Madupu, J. D. Peterson, L. A. Umayam, O. White, A. M. Wolf, J. Vamathevan, J. Weidman, M. Impraim, K. Lee, K. Berry, C. Lee, J. Mueller, H. Khouri, J. Gill, T. R. Utterback, L. A. McDonald, T. V. Feldblyum, H. O. Smith, J. C. Venter, K. H. Nealson, and C. M. Fraser, *Nat. Biotechnol.*, 2002, **20**, 1118–23.
2. D. Coursolle and J. A. Gralnick, *Mol. Microbiol.*, 2010, **77**, 995–1008.
3. R. S. Hartshorne, C. L. Reardon, D. Ross, J. Nuester, T. a Clarke, A. J. Gates, P. C. Mills, J. K. Fredrickson, J. M. Zachara, L. Shi, A. S. Beliaev, M. J. Marshall, M. Tien, S. Brantley, J. N. Butt, and D. J. Richardson, *Proc. Natl. Acad. Sci. U. S. A.*, 2009, **106**, 22169–74.
4. J. K. Fredrickson, M. F. Romine, A. S. Beliaev, J. M. Auchtung, M. E. Driscoll, T. S. Gardner, K. H. Nealson, A. L. Osterman, G. Pinchuk, J. L. Reed, D. A. Rodionov, J. L. M. Rodrigues, D. A. Saffarini, M. H. Serres, A. M. Spormann, I. B. Zhulin, and J. M. Tiedje, *Nat. Rev. Microbiol.*, 2008, **6**, 592–603.
5. D. H. Park and B. H. Kim, 2001, **39**, 273–278.
6. D. J. Richardson, J. N. Butt, J. K. Fredrickson, J. M. Zachara, L. Shi, M. J. Edwards, G. White, N. Baiden, A. J. Gates, S. J. Marritt, and T. A. Clarke, 2012, **85**, 201–212.
7. J. Du, C. Catania, and G. Bazan, *Chem. Mater.*, 2013, **26**, 686–697.
8. D. R. Lovley, *Annu. Rev. Microbiol.*, 2012, **66**, 391–409.
9. B. E. Logan, *Nat. Rev. Microbiol.*, 2009, **7**, 375–81.
10. A. E. Franks and K. P. Nevin, *Energies*, 2010, **3**, 899–919.
11. J. N. Roy, S. Babanova, K. E. Garcia, J. Cornejo, L. K. Ista, and P. Atanassov, *Electrochim. Acta*, 2013, 1–8.
12. C. R. Myers and J. M. Myers, *J. Bacteriol.*, 1992, **174**, 3429–3438.
13. L. Shi, B. Chen, Z. Wang, D. A. Elias, M. U. Mayer, Y. A. Gorby, S. Ni, B. H. Lower, D. W. Kennedy, D. S. Wunschel, H. M. Mottaz, M. J. Marshall, E. A. Hill, A. S. Beliaev, J. M. Zachara, J. K. Fredrickson, and T. C. Squier, *J. Bacteriol.*, 2006, **188**, 4705–14.
14. R. S. Hartshorne, B. N. Jepson, T. A. Clarke, S. J. Field, J. Fredrickson, J. Zachara, L. Shi, J. N. Butt, and D. J. Richardson, *J. Biol. Inorg. Chem.*, 2007, **12**, 1083–94.
15. M. Firer-Sherwood, G. S. Pulcu, and S. J. Elliott, *J. Biol. Inorg.*

- Chem.*, 2008, **13**, 849–54.
16. D. Baron, E. LaBelle, D. Coursolle, J. A. Gralnick, and D. R. Bond, *J. Biol. Chem.*, 2009, **284**, 28865–73.
17. L. Shi, D. J. Richardson, Z. Wang, S. N. Kerisit, K. M. Rosso, J. M. Zachara, and J. K. Fredrickson, *Environ. Microbiol. Rep.*, 2009, **1**, 220–227.
18. A. Okamoto, R. Nakamura, and K. Hashimoto, *Electrochim. Acta*, 2011, **56**, 5526–5531.
19. A. Okamoto, K. Hashimoto, and R. Nakamura, 2012, **85**, 61–65.
20. M. J. Marshall, A. S. Beliaev, A. C. Dohnalkova, D. W. Kennedy, L. Shi, Z. Wang, M. I. Boyanov, B. Lai, K. M. Kemner, J. S. McLean, S. B. Reed, D. E. Culley, V. L. Bailey, C. J. Simonson, D. A. Saffarini, M. F. Romine, J. M. Zachara, and J. K. Fredrickson, *PLoS Biol.*, 2006, **4**, e268.
21. E. Marsili, D. B. Baron, I. D. Shikhare, D. Coursolle, J. A. Gralnick, and D. R. Bond, *Proc. Natl. Acad. Sci. U. S. A.*, 2008, **105**, 3968–73.
22. H. von Canstein, J. Ogawa, S. Shimizu, and J. R. Lloyd, *Appl. Environ. Microbiol.*, 2008, **74**, 615–23.
23. E. D. Brutinel and J. A. Gralnick, *Appl. Microbiol. Biotechnol.*, 2012, **93**, 41–8.
24. R. Li, J. M. Tiedje, C. Chiu, and R. M. Worden, *Environ. Sci. Technol.*, 2012, **46**, 2813–20.
25. N. J. Kotloski and J. A. Gralnick, *MBio*, 2013, **4**, 1–4.
26. C. Léger and P. Bertrand, *Chem. Rev.*, 2008, **108**, 2379–438.
27. D. E. Ross, S. L. Brantley, and M. Tien, *Appl. Environ. Microbiol.*, 2009, **75**, 5218–26.
28. A. Okamoto, K. Hashimoto, K. H. Neelson, and R. Nakamura, *Proc. Natl. Acad. Sci.*, 2013, **110**, 1–6.
29. D. Coursolle, D. B. Baron, D. R. Bond, and J. A. Gralnick, *J. Bacteriol.*, 2010, **192**, 467–74.
30. Y. A. Gorby, S. Yanina, J. S. McLean, K. M. Rosso, D. Moyles, A. Dohnalkova, T. J. Beveridge, I. S. Chang, B. H. Kim, K. S. Kim, D. E. Culley, S. B. Reed, M. F. Romine, D. A. Saffarini, E. A. Hill, L. Shi, D. A. Elias, D. W. Kennedy, G. Pinchuk, K. Watanabe, S. Ishii, B. Logan, K. H. Neelson, and J. K. Fredrickson, *Proc. Natl. Acad. Sci. U. S. A.*, 2006, **103**, 11358–63.
31. M. Y. El-Naggar, G. Wanger, K. M. Leung, T. D. Yuzvinsky, G. Southam, J. Yang, W. M. Lau, K. H. Neelson, and Y. a Gorby, *Proc. Natl. Acad. Sci. U. S. A.*, 2010, **107**, 18127–31.
32. S. M. Strycharz-Glaven, R. M. Snider, A. Guiseppi-Elie, and L. M. Tender, *Energy Environ. Sci.*, 2011, **4**, 4366.
33. N. F. Polizzi, S. S. Skourtis, and D. N. Beratan, *Faraday Discuss.*, 2012, **155**, 43.
34. S. Pirbadian and M. Y. El-Naggar, *Phys. Chem. Chem. Phys.*, 2012, **14**, 13802–8.
35. L. A. Fitzgerald, E. R. Petersen, R. I. Ray, B. J. Little, C. J. Cooper, E. C. Howard, B. R. Ringeisen, and J. C. Biffinger, *Process Biochem.*, 2012, **47**, 170–174.
36. N. S. Malvankar and D. R. Lovley, *ChemSusChem*, 2012, **5**, 1039–1046.
37. N. S. Malvankar, M. T. Tuominen, and D. R. Lovley, *Energy Environ. Sci.*, 2012, **5**, 6247.
38. L. E. Garner, J. Park, S. M. Dyar, A. Chworos, J. J. Sumner, and G. C. Bazan, *J. Am. Chem. Soc.*, 2010, **132**, 10042–52.
39. H. Hou, X. Chen, A. W. Thomas, C. Catania, N. D. Kirchofer, L. E. Garner, A. Han, and G. C. Bazan, *Adv. Mater.*, 2013, 1–5.
40. V. B. Wang, J. Du, X. Chen, A. W. Thomas, N. D. Kirchofer, L. E. Garner, M. T. Maw, W. H. Poh, J. Hinks, S. Wuertz, S. Kjelleberg, Q. Zhang, J. S. C. Loo, and G. C. Bazan, *Phys. Chem. Chem. Phys.*, 2013, **15**, 5867–72.
41. L. E. Garner, A. W. Thomas, J. J. Sumner, S. P. Harvey, and G. C. Bazan, *Energy Environ. Sci.*, 2012, **5**, 9449.
42. A. W. Thomas, L. E. Garner, K. P. Nevin, T. L. Woodard, A. E. Franks, D. R. Lovley, J. J. Sumner, C. J. Sund, and G. C. Bazan, *Energy Environ. Sci.*, 2013, **6**, 1761.
43. H. Y. Woo, B. Liu, B. Kohler, D. Korystov, A. Mikhailovsky, and G. C. Bazan, *J. Am. Chem. Soc.*, 2005, **127**, 14721–14729.
44. Y. Lee, I. Yang, J. E. Lee, S. Hwang, J. W. Lee, S. Um, T. L. Nguyen, P. J. Yoo, H. Y. Woo, J. Park, and S. K. Kim, *J. Phys. Chem. C*, 2013, **117**, 3298–3307.
45. J. Du, A. W. Thomas, X. Chen, L. E. Garner, C. a Vandenberg, and G. C. Bazan, *Chem. Commun. (Camb.)*, 2013, **49**, 9624–6.
46. J. Hinks, Y. Wang, W. H. Poh, B. C. Donose, A. W. Thomas, S. Wuertz, S. C. J. Loo, G. C. Bazan, S. L. A. Kjelleberg, Y. Mu, and T. W. Seviour, *Langmuir*, 2014.
47. V. B. Wang, N. D. Kirchofer, X. Chen, M. Y. L. Tan, K. Sivakumar, B. Cao, Q. Zhang, S. Kjelleberg, G. C. Bazan, S. C. J. Loo, and E. Marsili, *Electrochem. commun.*, 2014, **41**, 55–58.
48. Y. J. Tang, A. L. Meadows, and J. D. Keasling, *Biotechnol. Bioeng.*, 2007, **96**, 125–133.
49. R. Renslow, J. Babauta, A. Kuprat, J. Schenk, C. Ivory, J. Fredrickson, and H. Beyenal, *Phys. Chem. Chem. Phys.*, 2013, **15**, 19262–83.
50. F. A. Armstrong, H. A. Heering, and J. Hirst, *Chem. Soc. Rev.*, 1997, **26**, 169–179.
51. E. Marsili, J. B. Rollefson, D. B. Baron, R. M. Hozalski, and D. R. Bond, *Appl. Environ. Microbiol.*, 2008, **74**, 7329–37.
52. A. Jain, X. Zhang, G. Pastorella, J. O. Connolly, N. Barry, R. Woolley, S. Krishnamurthy, and E. Marsili, *Bioelectrochemistry*, 2012, **87**, 28–32.
53. Z. Zhou and R. P. Swenson, *Biochemistry*, 1996, **35**, 15980–15988.
54. A. J. Bard and L. R. Faulkner, *Electrochemical Methods: Fundamentals and Applications*, 2nd edn., 2001.
55. B. Cao, L. Shi, R. N. Brown, Y. Xiong, J. K. Fredrickson, M. F. Romine, M. J. Marshall, M. S. Lipton, and H. Beyenal, *Environ. Microbiol.*, 2011, **13**, 1018–31.
56. B. H. Lower, R. Yongsunthon, L. Shi, L. Wildling, H. J. Gruber, N. S. Wigginton, C. L. Reardon, G. E. Pinchuk, T. C. Droubay, J.-F. Boily, and S. K. Lower, *Appl. Environ. Microbiol.*, 2009, **75**, 2931–5.